UNIVERSITY OF BUCHAREST
FACULTY OF CHEMISTRY
DOCTORAL SCHOOL IN CHEMISTRY

DOCTORAL THESIS

MOLECULAR MAGNETIC MATERIALS CONSTRUCTED USING NITRONYL NITROXIDE RADICALS

ABSTRACT

PhD Student:
Cristian Andrei Spînu

Scientific Supervisor:
Acad. Marius Andruh

2026

The PhD thesis with the title "Molecular magnetic materials constructed using nitronyl nitroxide radicals" proposed as its main objective the research towards the synthesis of novel coordination compounds containing nitronyl nitroxide radicals as ligands, and the investigation of their crystalline structures and magnetic properties.

The thesis was divided in seven chapters with the first three chapters dedicated to the theoretical part.

Chapter I describes the classification of radicals, taking into account their chemical reactivity, in *transient*, *persistent* and *stable* radicals.[1,2,3] It further discusses conceptually the use of different steric constrains or electron donating and electron withdrawing groups in order to increase the stability of the organic radical. In this context, the nitronyl nitroxide stable radicals are depicted in detail. Nitronyl nitroxides were firstly obtained by Ullman in 1968,[4,5] and are synthesized via a condensation reaction between an alkyl or aryl aldehyde with 2,3-bis(hydroxylamino)-2,3-dimethylbutane **9**, to obtain the imidazolidine intermediate, which is further oxidized with lead dioxide, manganese dioxide, or sodium metaperiodate (figure 1).

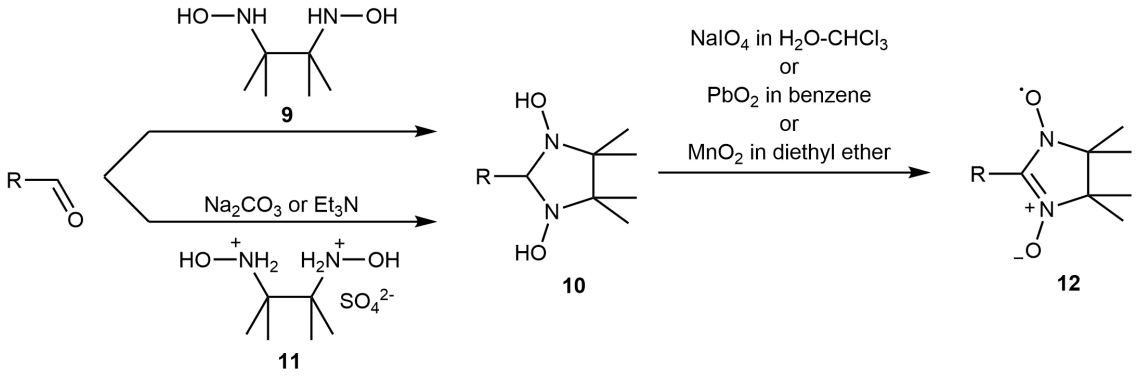


Figure 1. Synthesis of nitronyl nitroxide radicals.

Benzimidazole derived nitronyl nitroxides are obtained through a different synthetic route, by reacting *N*-phenylhydroxilamine and benzaldehyde to obtain a nitrone intermediate, which is further reacted with benzofuroxan, followed by an oxidation reaction.[6]

It is also possible to employ cross-coupling reactions to bind a nitronyl nitroxide moiety to organic substrates by using organometallic radical species and aryl halides (figure 2).[7]

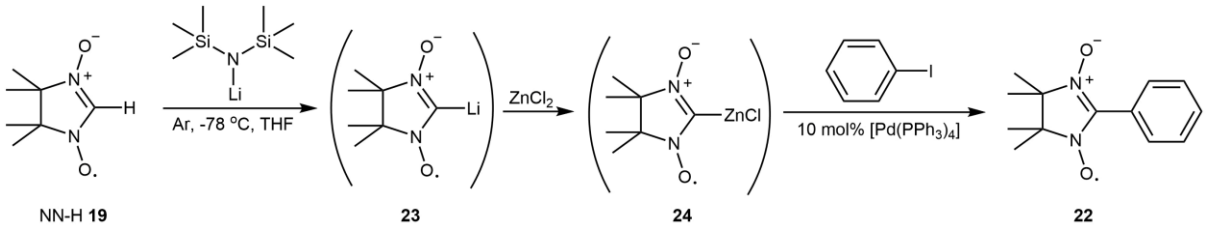


Figure 2. Cross-coupling reaction of iodobenzene with the organozinc radical **24** in the presence of $[Pd(PPh_3)_4]$ catalyst.

This chapter also reviews the synthetic procedures of the key precursor for nitronyl nitroxide radicals, 2,3-bis(hydroxylamino)-2,3-dimethylbutane **9**. The precursor **9** is obtained by a reduction reaction of the nitro groups within 2,3-dimethyl-2,3-dinitrobutane with zinc and ammonium chloride or with aluminium amalgam.[8,9]

The synthesis of novel nitronyl nitroxides requires new aldehydes which can be obtained by means of Duff reactions.[10] By using hexamethylenetetramine in the presence of trifluoracetic acid, a formyl group is introduced on phenolic substrates.[11,12]

Chapter II contains introductory information regarding the field of molecular magnetism and the field of molecular qubits. When molecules bearing unpaired electrons are subjected to a homogeneous magnetic field *H*, the magnetic moment of the electrons will tend to align in the direction of the magnetic field, obtaining a magnetisation *M*. There are cases when the molecules retain the magnetisation *M* in the absence of an external magnetic field *H*, describing a hysteresis loop. If this effect arises from the interactions of electrons within a molecule and not from a long range magnetic ordering between electrons from many molecules, we classify the molecule as a molecular magnet.[13,14,15,16,17,18] The magnetic properties of the first single molecular magnet where described in 1993 by Sessoli, Gatteschi *et al.*,[19] for the dodecanuclear manganese carboxylate mixed valence complex $[Mn^{IV}_4Mn^{III}_8(CH_3COO)_{16}(H_2O)_4O_{12}]\cdot 2CH_3COOH\cdot 4H_2O$, which exhibited a magnetic hysteresis at a temperature of 2.2 K. A similar behaviour was observed for the first single chain magnet, a one-dimensional coordination polymer $[Co(hfac)_2(\mathbf{32})]_\infty$ (figure 3), which was obtained by the reaction between *p*-methoxy-phenyl nitronyl nitroxide **32** and $Co(hfac)_2$ (hfac = hexafluoroacetylacetonate). Magnetic measurement performed on the single crystal of coordination polymer $[Co(hfac)_2(\mathbf{32})]_\infty$ revealed, at low temperatures, the presence of a hysteresis loop when the magnetic field was applied parallel to the chain axis, while no hysteresis is observed when the field was applied perpendicular to the chain axis (figure 4).

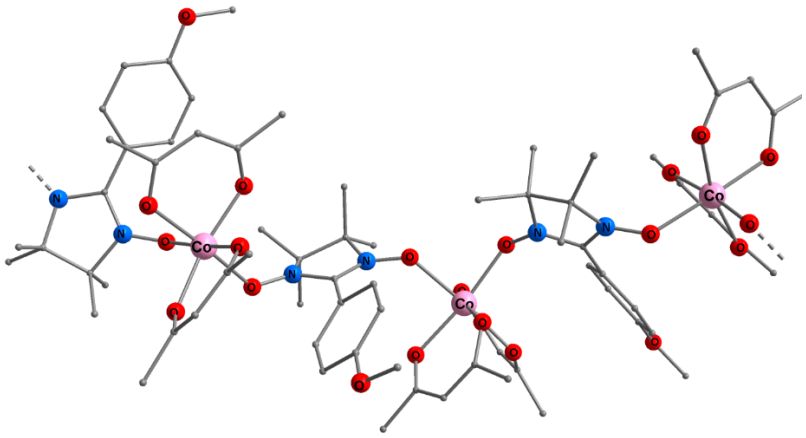


Figure 3. Crystal structure of the one-dimensional coordination polymer [Co(hfac)$_2$(**32**)]$_\infty$. Atom color code: cobalt pink, oxygen red, nitrogen blue and carbon gray, while hydrogen and fluorine atoms are omitted for clarity (adapted from ref. 19).

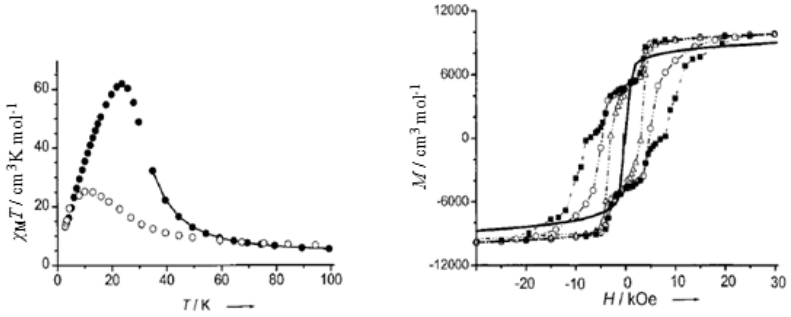


Figure 4. $\chi_M T$ product as a function of temperature measured in external field parallel (●) and perpendicular (○) to chain direction for [Co(hfac)$_2$(**32**)]$_\infty$ (left); Magnetisation hysteresis loop recorded at 2 - 4.5 K on a single crystal of [Co(hfac)$_2$(**32**)]$_\infty$ parallel to the chain and perpendicular to it (line) (right) (adapted form ref. 19).

A qubit is a physical element capable to carry information in a superposition of quantum states, and, by means of quantum logic may execute some calculation tasks with greater computation speeds than the classical counterpart. One such physical element is represented by paramagnetic molecules, which can work as qubits as they contain unpaired electrons with a spin quantum number (m_s = ±1/2) that can be manipulated by electromagnetic radiation as microwave pulses. In general the performance of a spin qubit is evaluated through two parameters which characterise the relaxation processes: (a) the spin-lattice relaxation time, T_1, which represents the time needed for the spin system to relax to a thermal equilibrium with the surrounding lattice and (b) the spin-spin relaxation time, T_2, which represents the quantum coherence time that controls the superposition lifetime and is associated with the time when computations may take place. Sometimes, in the place of spin-spin relaxation time, T_2, the

phase memory time constant, T_m, is used, which, besides the spin-spin relaxation, also takes into account other relaxation effects from spectral and instantaneous diffusions.[20,21,22] The T_2 time, at a temperature of 4.5 K, for the Cr_7Ni complex, $[Et_2NH_2][Cr_7NiF_8(Me_3CCO_2)_{16}]$, was found to be 370 ns, while, for a deuterated sample of the Cr_7Ni complex, it was determined to be 2210 ns, fact which suggested a decoherence mechanism arising from the interaction of the electron spin with nuclear moments of the nearby protons.[23]

Chapter III starts with the presentation of the most common coordination modes of the nitronyl nitroxide radical, which are: monodentate (a), μ_2-η^2 monodentate bridging (b), and μ_2-η^1-η^1 bidentate bridging (c) (figure 5). Further, the chapter reviews the literature for metal complexes containing nitronyl nitroxide ligands derived from phenols, categorising them as discrete entities. Selected examples of coordination polymers are discussed as well. The analysis focuses on the structural parameters of the coordination compounds and their magnetic properties.

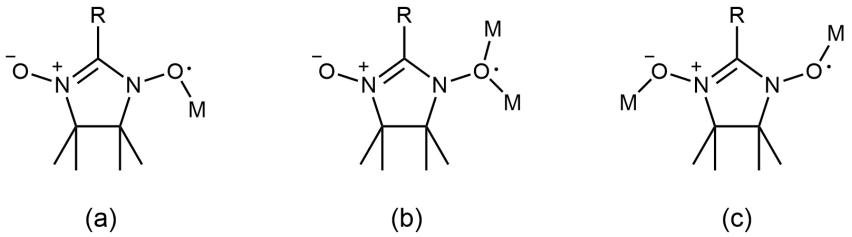


Figure 5. Coordination modes of nitronyl nitroxide radical.

The last four chapters were dedicated to the original contributions of the thesis.

Chapter IV describes the synthesis of the organic precursors followed by the synthesis of the nitronyl nitroxide radicals. The key precursor, 2,3-bis(hydroxylamino)-2,3-dimethylbutane **9**, was obtained upon the reduction of the nitro groups within 2,3-dimethyl-2,3-dinitrobutane **13** in the presence of Hg-Al amalgam (figure 6).[24] Following literally the steps described in the reported synthetic procedure,[24] does not always lead to a successful reaction, meaning that impactful minor details were not disclosed or described in depth. Thus, the reaction procedure was revisited and described with detailed steps. The yield of the reaction is influenced by the amalgamation of the aluminium and the temperature of the reaction medium during the reduction.

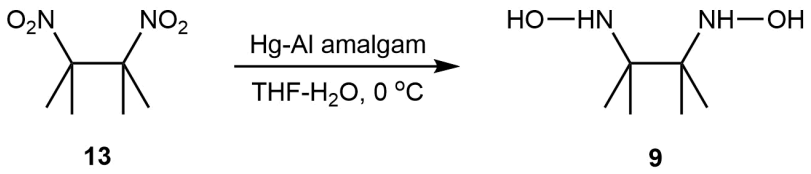


Figure. 6. Synthesis of 2,3-bis(hydroxylamino)-2,3-dimethylbutane **9**.

Further in the chapter, the synthesis of two new aldehydes derived from bisphenol A were described (figure 7). The aldehydes where prepared from the dinitro derivative of bisphenol A and hexametilenetetramine in trifluoroacetic acid, and they were isolated in pure form by column chromatography. The structures of the dialdehydes were proved by infrared and NMR spectroscopy, mass spectrometry, and, in the case of dialdehyde **52**, was also investigated by singe crystal X-ray diffraction (figure 8).

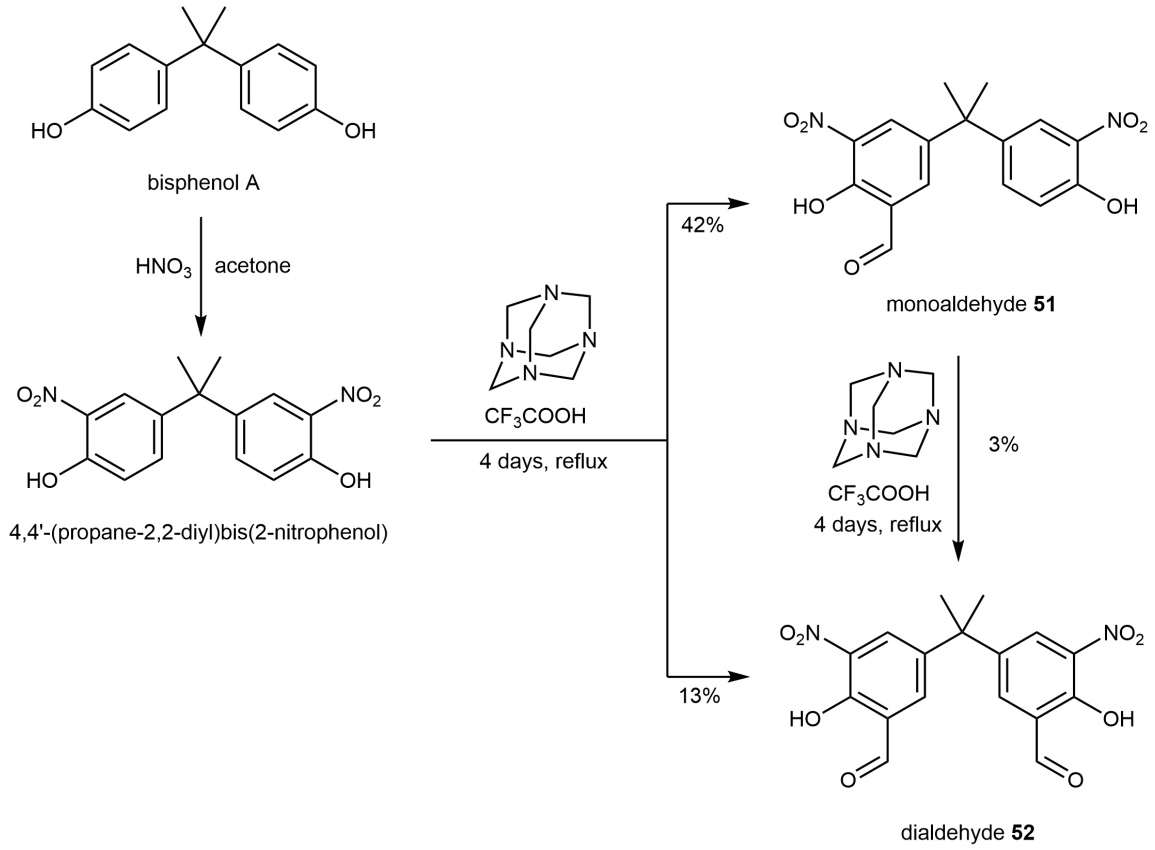


Figure 7. Synthesis of mono- and dialdehyde derived from bisphenol A.

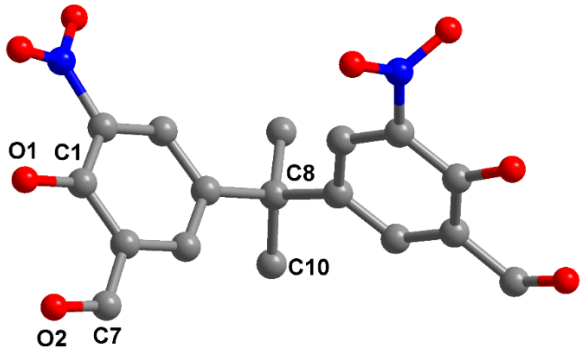


Figure 8. Molecular structure of dialdehyde **52**, with the atom colour code: carbon gray, oxygen red, nitrogen blue; hydrogen atoms were omitted for clarity.

Next, the synthesis of nitronyl nitroxide organic radicals where investigated and described in detail. The radicals were chosen in such way that they would carry the maximal number of electron withdrawing groups, conjugating groups, and electron donating groups, in order to increase, as much as possible, their stability, and, most importantly, their ability to bind coordinatively to metal ions. One of the synthesized radicals is the nitronyl nitroxide **54** (figure 9), which was obtained following the Ullman path.[4,5] Although a similar synthesis path for nitronyl nitroxide **54** was published by Ovcharenko *et. al.*,[25] the synthesis procedure described in this thesis generated the product in a higher yield, of 46%, and the procedure was scaled at grams quantity.

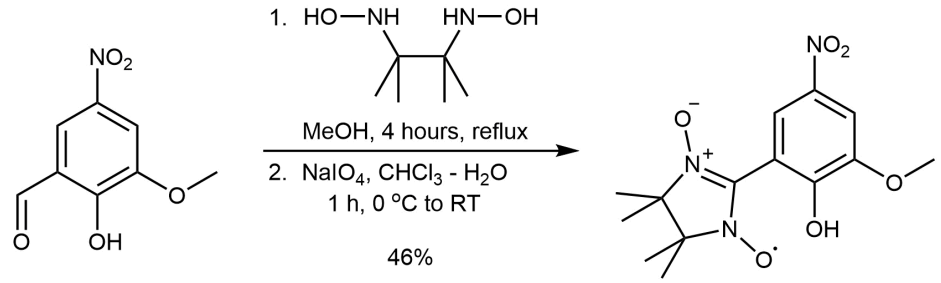


Figure 9. Synthesis of nitronyl nitroxide **54**.

The electron paramagnetic resonance spectrum (EPR) of nitronyl nitroxide **54** was also registered. The spectrum (figure 10) presents five lines, a pattern characteristic for nitronyl nitroxide radicals, which arises from the hyperfine splitting of the two quasi equivalent nitrogen atoms with a_{N1} = 7.40 G and a_{N2} = 7.55 G, and the determined unpaired electron *g* factor have value of 2.0053.

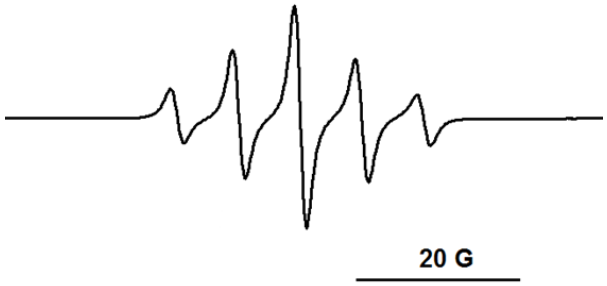


Figure 10. EPR spectrum of nitronyl nitroxide **54** recorded in dichloromethane at 293 K.

Another investigated molecule was the nitroxide diradical **55** (figure 11) which was synthesized by a condensation reaction between the dialdehyde **52** and 2,3-bis(hydroxylamino)-2,3-dimethylbutane **9**, followed by an oxidation reaction with $NaIO_4$. The nitronyl nitroxide **55** was isolated in pure form by column chromatography with an overall yield of 25%.

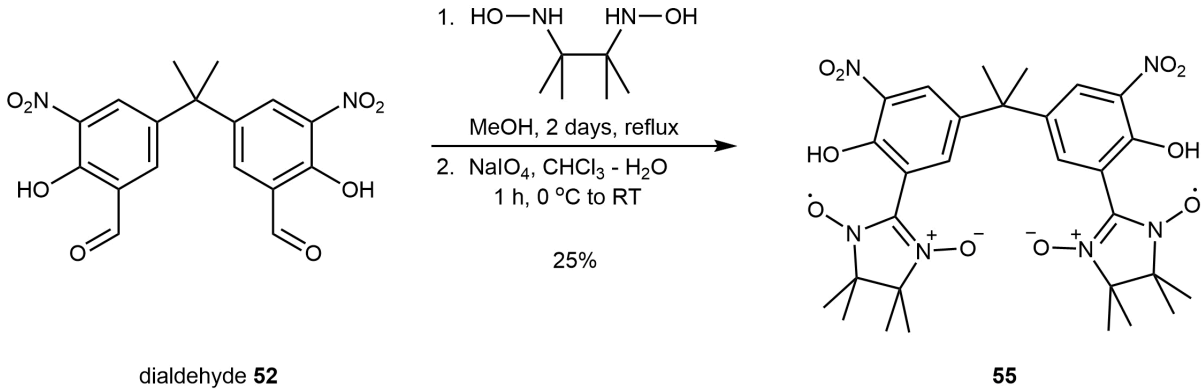


Figure 11. Nitronyl nitroxide **55** synthesis scheme.

The EPR spectrum of nitronyl nitroxide **55** (figure 12) was registered in different solvents. The spectrum displays more than five lines, an effect attributed to the spin-spin interaction of the two unpaired electrons. Due to the fact that the structure of the diradical **55** is flexible, the electron paramagnetic resonance spectrum registers the sum of the components corresponding to different conformations that bring the two paramagnetic groups at various distances. In consequence the experimental spectrum changes with temperature and solvent. The hyperfine splitting constants arising from the interaction of the unpaired electron with the nuclei of the two equivalent nitrogen atoms, $a_{N1} = a_{N2}$, are 7.45 G in toluene, 7.64 G in dichloromethane, and 8.20 G in water, and the determined *g* factor has a value of 2.0049.

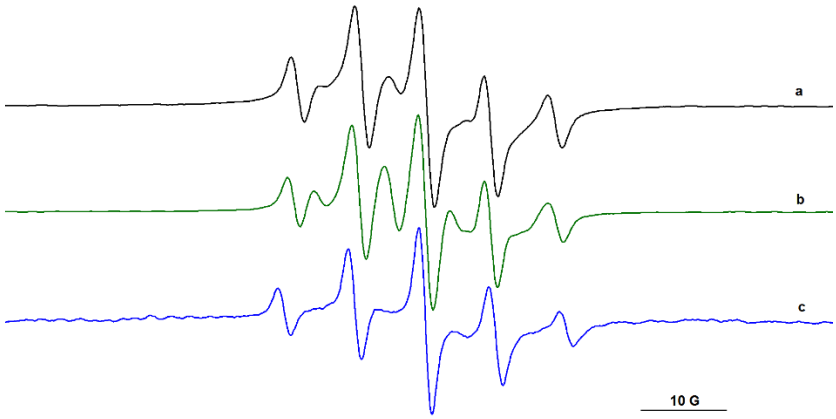


Figure 12. EPR spectra of nitronyl nitroxide **55** recorded in (a) toluene, (b) dichloromethane and (c) water at 295 K.

Chapter V of the thesis depicts the research towards the investigations of transition metal complexes obtained using nitronyl nitroxides **54** and **55**. The radical **54** derived from nitro-*o*-vanillin was reacted with transition metal hexafluoroacetylacetonates, $M(hfac)_2 \cdot 2H_2O$ (where M^{II}: Mn, Co, Ni, Zn) and led to isostructural mononuclear complexes (figure 13).

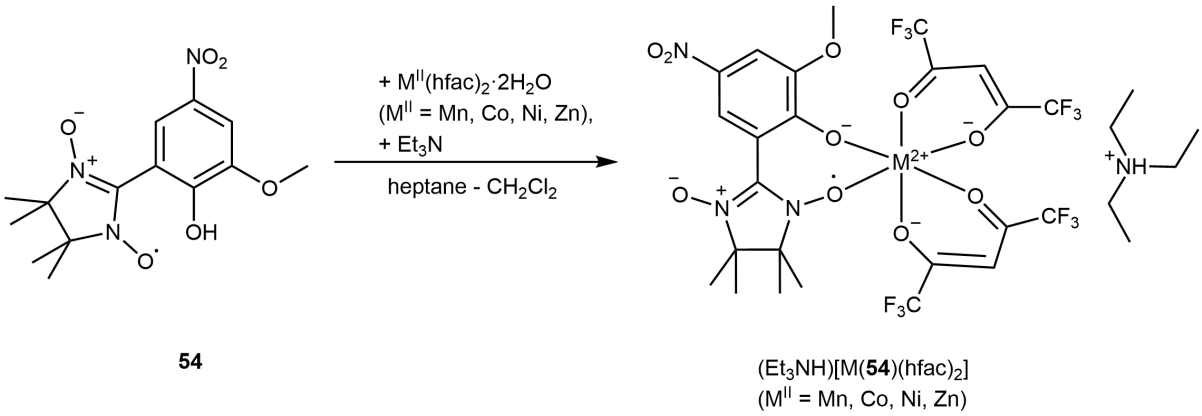


Figure 13. Synthesis diagram of $(Et_3NH)[M(\mathbf{54})(hfac)_2]$, where M = Mn, Co, Ni, Zn.

The single crystal X-ray measurements of the nickel compound revealed the presence of a complex anion $[Ni(\mathbf{54})(hfac)_2]^-$, in which the nickel ion presents an octahedral geometry and establish a direct bond to the radical moiety, as well as a triethylammonium cation (figure 14).

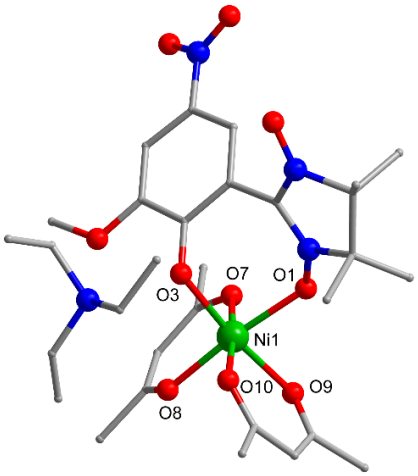


Figure 14. X-ray structure of the mononuclear complex $(Et_3NH)[Ni(\mathbf{54})(hfac)_2]$ with the atom colour code: nickel green, carbon gray, oxygen red, nitrogen blue; hydrogen and fluorine atoms were omitted for clarity.

The magnetic properties of the mononuclear complex $(Et_3NH)[Ni(\mathbf{54})(hfac)_2]$ were also investigated, and revealed a strong antiferromagnetic interaction between the Ni^{II} and the nitronyl nitroxide radical, resulting in a spin state of $S = 1/2$ under 120 K (figure 15). The fitting of the data with an isotropic spin Hamiltonian $H = -JS_{Ni}S_{Rad}$ yielded an exchange interaction constant $J = -351$ cm^{-1}, for which the sign and magnitude were confirmed by DFT calculations. The $S = 1/2$ spin state was further confirmed by the EPR investigation at 120 K with a $g = 2.2751$ in solution and $g = 2.2897$ for the solid sample. EPR spectra show the localisation of the electron spin on the Ni^{II} ion, however the DFT calculation hints towards some degree of delocalisation on the radical moiety.

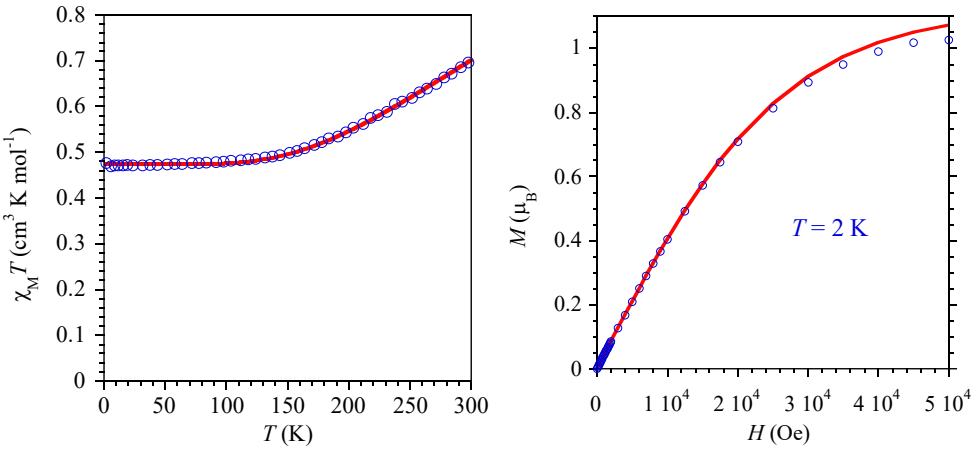


Figure 15. $\chi_M T$ vs T plot (left) and magnetisation vs applied magnetic field plot (right) for $(Et_3NH)[Ni(\mathbf{54})(hfac)_2]$ complex, with experimental data depicted in (O) and calculated data depicted in (-).

Further, the chapter describes the reactions of nitronyl nitroxide biradical **55** towards transition metal hexafluoroacetylacetonates, $M(hfac)_2 \cdot 2H_2O$ (where M^{II}: Co, Ni) which led to dinuclear complexes (figure 16).

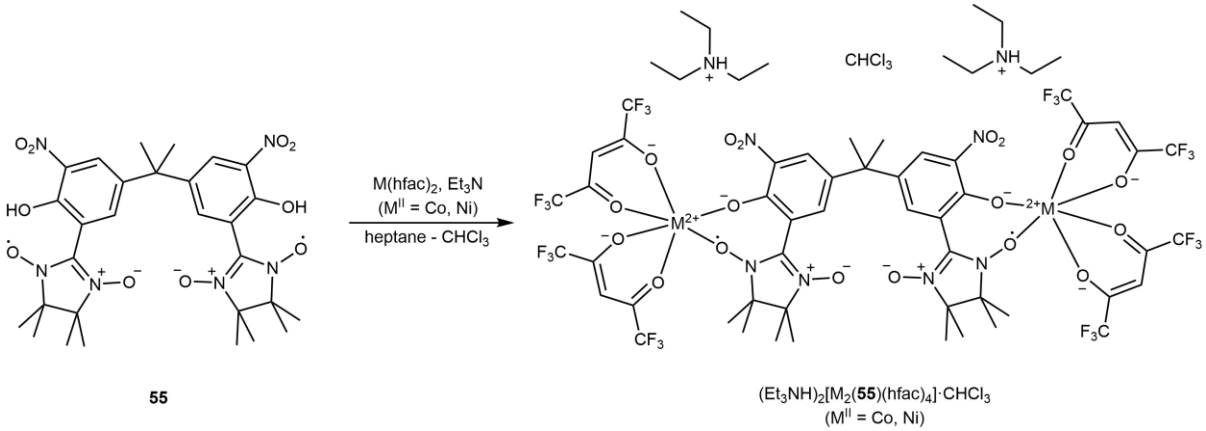


Figure 16. Synthesis diagram of $(Et_3NH)_2[M_2(\mathbf{55})(hfac)_4]\cdot CHCl_3$, where M = Co, Ni.

Single crystal X-ray diffraction measurements for the nickel complex, $(Et_3NH)_2[Ni_2(\mathbf{55})(hfac)_4]\cdot CHCl_3$, revealed a dinuclear compound, with the nickel ions in an octahedral geometry within an anionic dinuclear species $[Ni_2(\mathbf{55})(hfac)_4]^{2-}$, two triethylammonium cations Et_3NH^+ and one molecule of chloroform (figure 17).

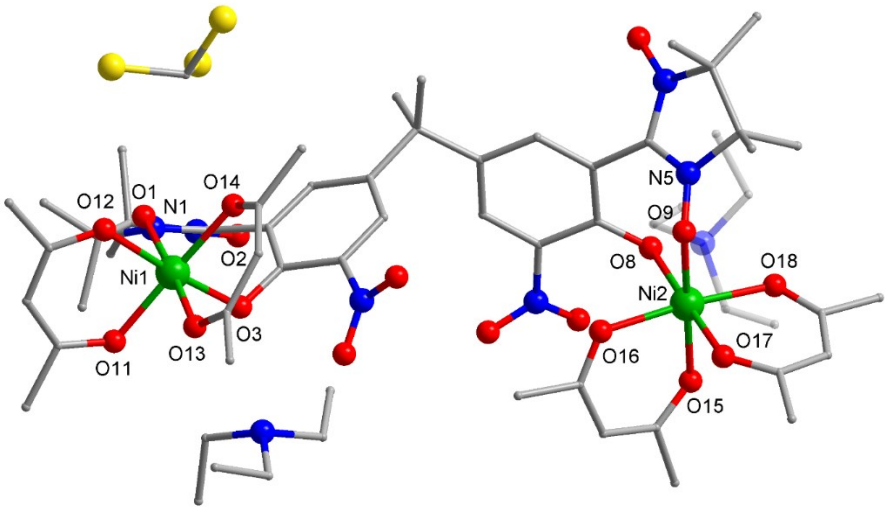


Figure 17. X-ray structure of $(Et_3NH)_2[M_2(\mathbf{55})(hfac)_4]\cdot CHCl_3$, where M = Co, Ni, with the atom colour code: nickel green, carbon gray, oxygen red, nitrogen blue; hydrogen and fluorine atoms were omitted for clarity.

The cryomagnetic investigation of the $(Et_3NH)_2[Ni_2(\mathbf{55})(hfac)_4]\cdot CHCl_3$ complex revealed a strong antiferromagnetic interaction between Ni^{II} and the nitronyl nitroxide radical

(figure 18). The data fitting, with an anisotropic Hamiltonian $\hat{H} = -J\hat{S}_1\hat{S}_2 + \mu_B\overrightarrow{B}(g_1\hat{S}_1 + g_2\hat{S}_2) + D_1(\hat{S}_{1,z}^2 - \frac{1}{3}S_1(S_1+1) + E_1(\hat{S}_{1,x}^2 - \hat{S}_{1,y}^2))$, yielded an exchange interaction constant J = -294.8 cm^{-1}, for which the sign and magnitude were confirmed by DFT calculations. Further, the DFT calculation revealed that the spin density is mainly localized on the Ni^{II} metal ion and to a lesser extent on the nitronyl nitroxide moiety.

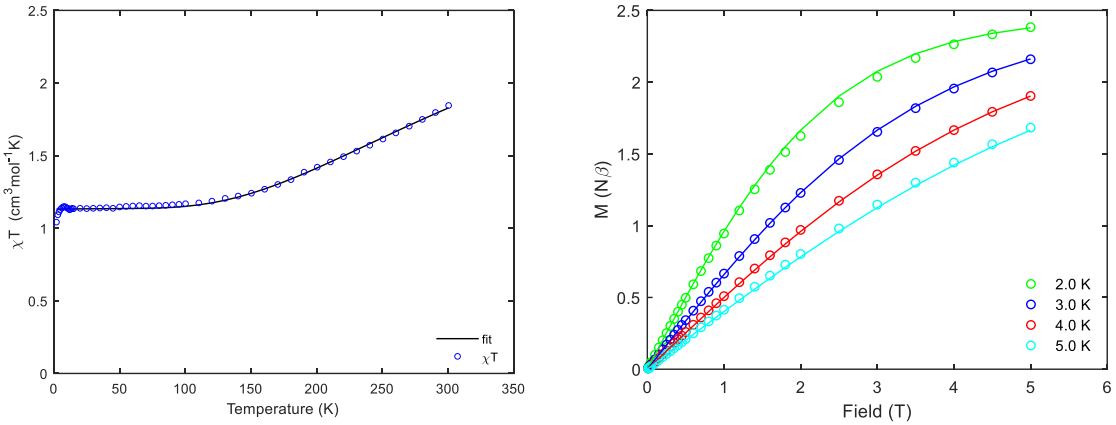


Figure 18. Magnetic susceptibility times temperature vs temperature plot (left) and magnetisation vs applied magnetic field plot (right) for $(Et_3NH)_2[Ni_2(\mathbf{55})(hfac)_4]\cdot CHCl_3$.

The **Chapter VI** details the research involved in obtaining 2*p*-4*f* heterodispin and 2*p*-3*d*-4*f* heterotrispin complexes. The reaction of nitronyl nitroxide radical derived from nitro-*o*-vanillin **54** towards Gd^{III}, Tb^{III}, and Dy^{III} hexafluoroacetylacetonato precursors resulted in the formation of three new tetranuclear complexes $(Et_3NH)[Ln_4(\mathbf{54\text{-}NN})(\mathbf{54\text{-}IN})(hfac)_6(CF_3COO)(\mu_3\text{-}OH)_4]$, where Ln^{III}: Gd^{III}, Tb^{III}, Dy^{III} (figure 19). The X-ray analysis revealed that all complexes are isostructural, with a distorted heterocubane cluster $\{Ln_4(\mu_3\text{-}OH)_4\}$ in which two lanthanide ions are eight coordinated, described by a square antiprism geometry, while the other two are nine coordinated, described by a spherical tricapped trigonal prism geometry (figure 20). Two radicals are distributed on the left and right sides of the complex, but the crystal structure data revealed that half of them are nitronyl nitroxide radicals and half of them are imino nitroxide radicals, with the latter being produced during the formation of the metal complex. Also, a trifluoroacetate anion is present in the structure, and it was formed in a retro Claisen condensation of part of the hexafluoroacetylacetonato ligands.

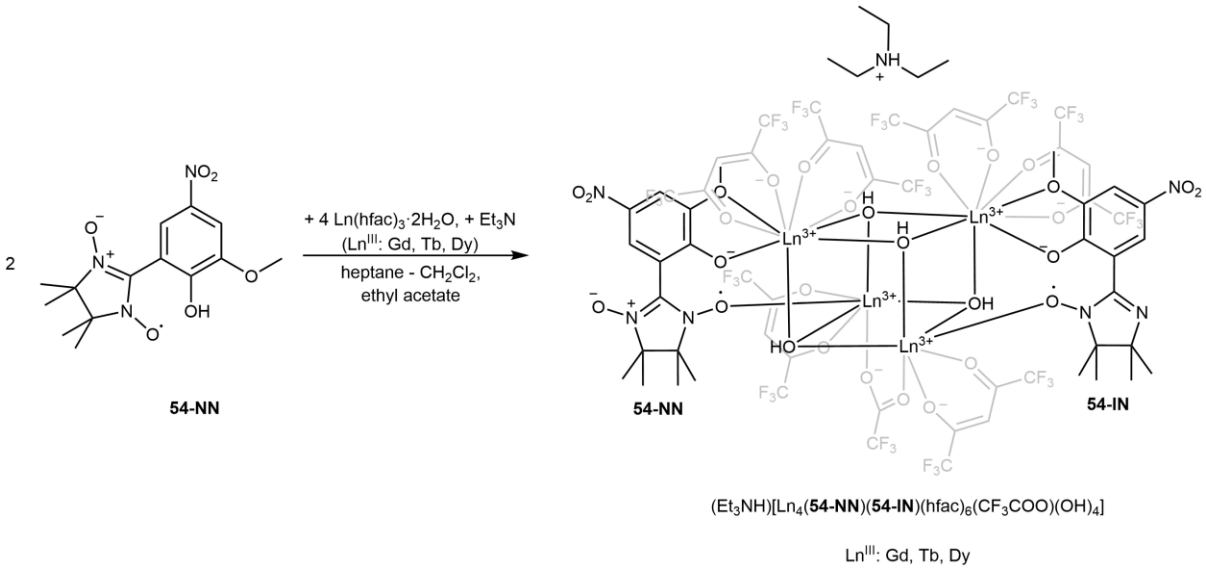


Figure 19. Synthesis diagram of $(Et_3NH)[Ln_4(\mathbf{54\text{-}NN})(\mathbf{54\text{-}IN})(hfac)_6(CF_3COO)(\mu_3\text{-}OH)_4]$, were Ln^{III}: Gd^{III}, Tb^{III}, Dy^{III}.

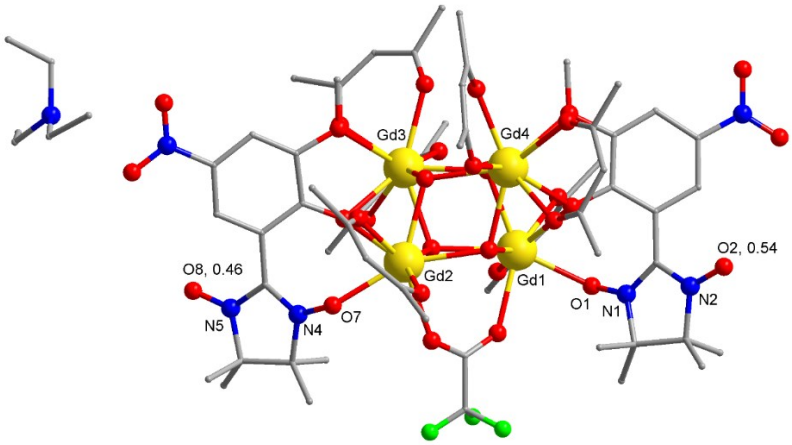


Figure 20. X-ray crystal structure of $(Et_3NH)[Gd_4(\mathbf{54\text{-}NN})(\mathbf{54\text{-}IN})(hfac)_6(CF_3COO)(\mu_3\text{-}OH)_4]$ with the atom colour code: gadolinium yellow, carbon gray, oxygen red, nitrogen blue, fluorine green; hydrogen and part of fluorine atoms were omitted for clarity.

The SQUID magnetometry investigation of $(Et_3NH)[Ln_4(\mathbf{54\text{-}NN})(\mathbf{54\text{-}IN})(hfac)_6(CF_3COO)(\mu_3\text{-}OH)_4]$, where Ln^{III}: Gd^{III}, Tb^{III}, Dy^{III}, suggests an antiferromagnetic behaviour of the heterocubane clusters, exemplified in the figure 21 for the Gd^{III} heterocubane.

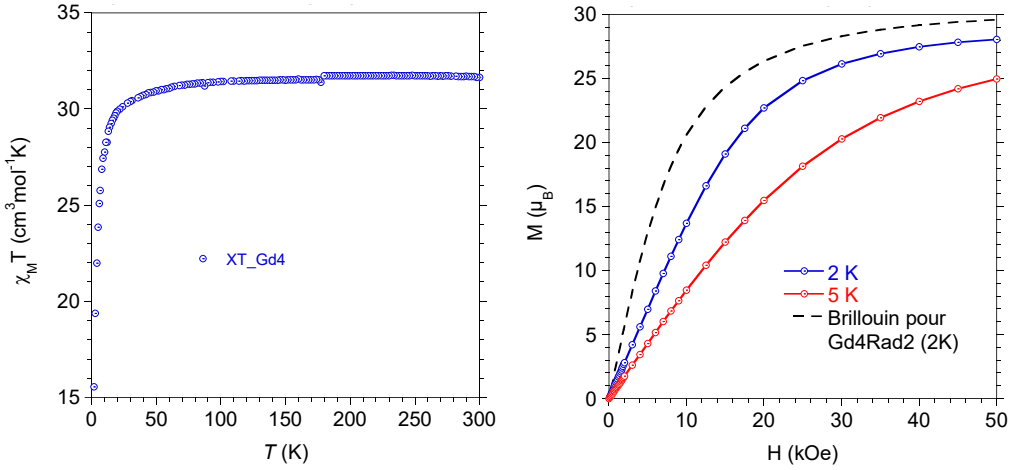


Figure 21. $\chi_M T$ product versus temperature (left) and magnetisation versus applied field (right) for **Gd_4** tetranuclear complex.

Further in this chapter, the complexation of the nitronyl nitroxide radical derived from nitro-*o*-vanillin **54** was studied towards a mixture of Ln^{III} (Gd^{III}, Tb^{III}, Dy^{III}) and Ni^{II} hexafluroacetylacetonates, generating a new family of 2*p*-3*d*-4*f* hetero-tri-spin trinuclear complexes, $[Ln_2Ni(\mathbf{54\text{-}IN})_2(hfac)_4(CF_3COO)_2]$ (figure 22).

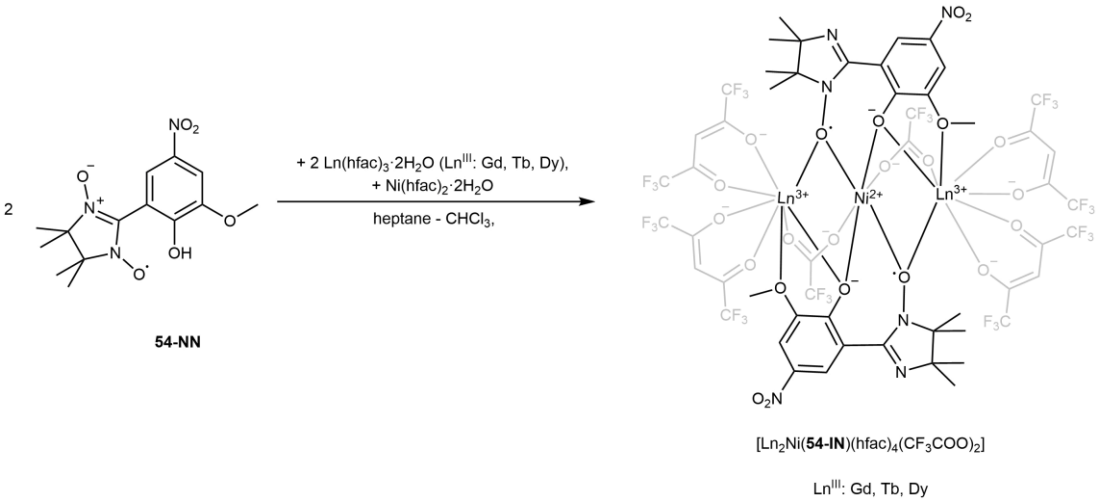


Figure 22. Synthesis diagram of $[Ln_2Ni(\mathbf{54\text{-}IN})_2(hfac)_4(CF_3COO)_2]$, where Ln^{III}: Gd^{III}, Tb^{III}, Dy^{III}.

Within the X-ray single crystal structure of $[Ln_2Ni(\mathbf{54\text{-}IN})_2(hfac)_4(CF_3COO)_2]$, where Ln^{III}: Gd, Tb, Dy, the nickel ion is six coordinated describing an octahedral geometry, while the lanthanide ions are eight coordinated describing a triangular dodecahedron geometry (figure 23). A similar situation regarding the reduction of nitronyl nitroxide radicals to imino nitroxide radicals has been also observed in the case of these complexes. Part of the hexafluoroacetylacetonato ligands participated to a retro Claisen condensation to form two trifluoroacetate anions. The fresh good crystals of the trinuclear compounds, after isolation

from the mother liquor, degrade by becoming mattified, processes in which the void volume in the good crystals decreased to a smaller void volume identified in the mattified crystals.

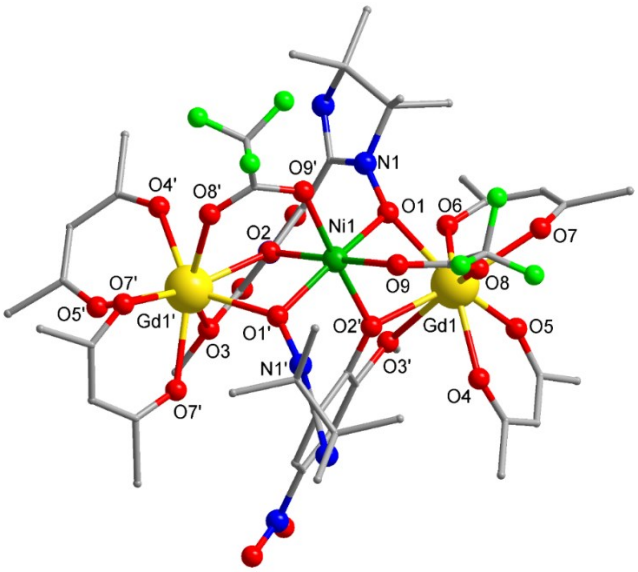


Figure 23. X-ray crystal structure of $[Gd_2Ni(\mathbf{54\text{-}IN})_2(hfac)_4(CF_3COO)_2]$ (**Gd_2Ni**) with the atom colour code: gadolinium yellow, carbon gray, oxygen red, nitrogen blue, fluorine green; hydrogen and part of fluorine atoms were omitted for clarity. The symmetry operation for Gd1' is 1-x, y, 1.5-z.

The SQUID magnetometry investigation of the $[Ln_2Ni(\mathbf{54\text{-}IN})_2(hfac)_4(CF_3COO)_2]$ complexes, where Ln^{III}: Gd^{III}, Tb^{III}, Dy^{III}, indicates dominant ferromagnetic interactions (figure 24).

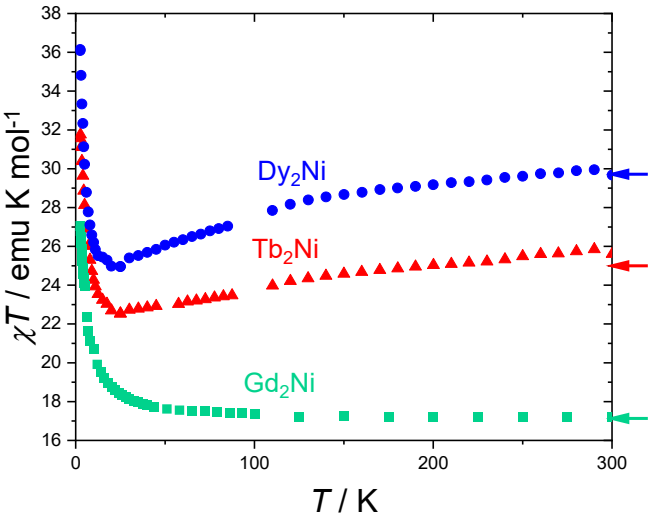


Figure 24. $\chi_M T$ product versus temperature plots for **Gd_2Ni** (green), **Tb_2Ni** (red), and **Dy_2Ni** (blue) registered under an applied field of 0.1 T, with the arrows indicating the Curie constant for magnetically independent spins.

Chapter VII describes the qubit behaviour of the two mononuclear complexes (Et_3NH)[Zn(**54**)$(hfac)_2$] and (Et_3NH)[Ni(**54**)$(hfac)_2$] with a $S = 1/2$ ground state as investigated by pulsed electron paramagnetic resonance (EPR).

The spin-lattice relaxation time T_1 for the zinc metal complex is quite long, with a value of 4.1 ms at 5.2 K, which decreases to a value of 197 μs at 100 K, while the phase memory time T_m is almost independent with the variation of the temperature, having a value of around 1.50 μs under 80 K, and a value close to 1 μs at 100 K, with the longest memory time displaying a value of 1.78 μs at 5 K (figure 25, a).

In the case of the nickel metal complex, T_1 is shorter, with a value of 0.5 ms at 5.5 K, which decreases to a value of 0.9 μs at 100 K, while the phase memory time T_m is independent with the variation of the temperature only under 30 K, with a value of approximatively 3 μs, and a value of 0.12 μs at 100 K and the longest memory time displaying a value of 3.7 μs at 5 K (figure 25, b). Overall the data suggests that the hyperfine couplings with the ligands nuclei play a significant role in spin relaxation.[26]

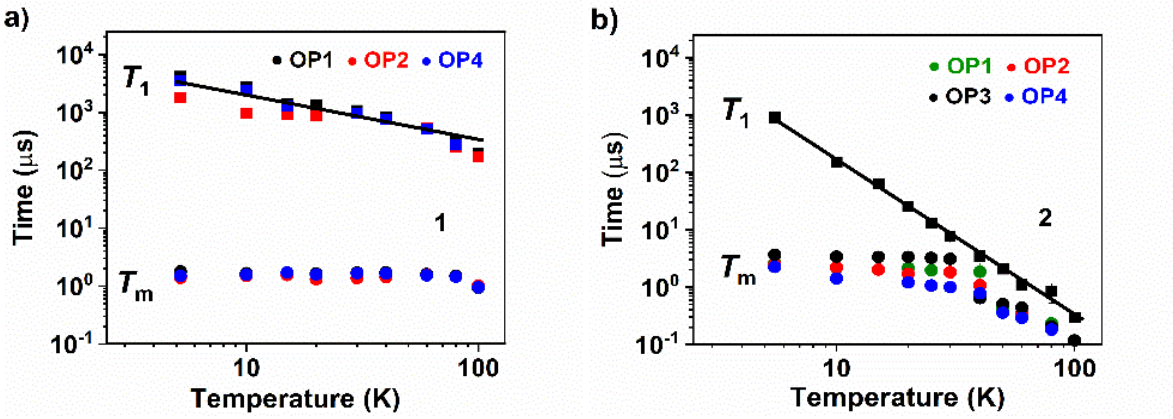


Figure 25. Spin lattice relaxation time T_1 and phase memory time T_m versus temperature for (Et_3NH)[Zn(**54**)$(hfac)_2$] (a) and (Et_3NH)[Ni(**54**)$(hfac)_2$] (b) metal complexes. The black line is a fit of al T_1 data with $T_1 = (aT + bT^n)^{-1}$.

Transient nutation experiments revealed coherent Rabi oscillations, which allowed the determination of the qubit operation time of 71 ns for the zinc compound and 72 ns for the nickel compound at 16 dB attenuation, and 12 ns at 1 dB (figure 26). This decrease suggests that the operation time is heavily diminished at higher power pulses. The figure of merit Q_M, equal to $2T_m\Omega_R$, which assesses the qubit performance, was calculated to be 134 for the zinc complex and 271 for the nickel complex.

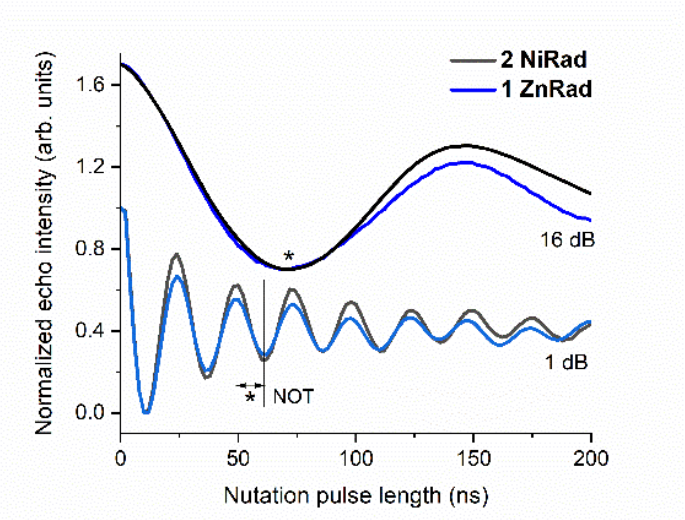


Figure 26. Rabi oscillations of $(Et_3NH)[Zn(\mathbf{54})(hfac)_2]$ (blue) and $(Et_3NH)[Ni(\mathbf{54})(hfac)_2]$ (black) acquired at microwave attenuation of 16 dB (top) and 1 dB (bottom) registered at 10 K, highlighting the "NOT-gate" single-qubit logic operation times (*).

During the research employed by the present thesis, synthetic procedures were revisited and improved while new precursors and nitronyl nitroxide radicals were synthesized. The obtained ligands generated novel heterospin metal complexes with intriguing magnetic properties, and two of the compounds displayed promising qubit properties.

The extensive research data was organised in eight annexes, containing comprehensive details on synthetic procedures, elemental analysis, infrared and UV-VIS spectra, nuclear magnetic resonance analysis, mass spectrometry, as well as crystallographic data and X-ray powder diffractograms.

Within the original findings of this doctoral thesis, **5** new organic molecules and **14** new coordination compounds were synthesised and characterised, and **3** synthetic procedures were revisited. Two compounds stimulated further research on their qubit properties. Part of the results of this research has been disseminated through four research articles:

1. Synthesis, crystal structure, magnetic, spectroscopic, and theoretical investigations of two new nitronyl-nitroxide complexes, **Cristian Andrei Spinu**, Céline Pichon, Gabriela Ionita, Teodora Mocanu, Sergiu Calancea, Mihai Raduca, Jean-Pascal Sutter, Mihaela Hillebrand, Marius Andruh, *Journal of Coordination Chemistry*, **2021**, *74*, 279-293. https://doi.org/10.1080/00958972.2021.1871900

   IF = 1.869

2. Two new 2p–3d metal complexes with a nitronyl-nitroxide ligand derived from *o*-vanillin: synthesis, crystals structures and magnetic properties, **Cristian Andrei Spinu**, Daniel O. T. A. Martins, Teodora Mocanu, Mihaela Hillebrand, Jean-Pascal Sutter, Floriana Tuna, Marius Andruh, *Magnetochemistry*, **2024**, *10*, 86.
https://doi.org/10.3390/magnetochemistry10110086

IF = 2.5

3. Design of a new nitronyl-nitroxide biradical and its complexes: synthesis, crystal structures and magnetic properties, **Cristian Andrei Spinu**, Ghenadie Novitchi, Mihaela Hillebrand, Teodora Mocanu, Gabriela Ionita, Anamaria Hanganu, Victorita Tecuceanu, Marius Andruh, *CrystEngComm*, **2025**, *27*, 6462-6472.
https://doi.org/10.1039/D5CE00795J

IF = 2.6

4. Investigation of hyperfine interactions in molecular spin qubits constructed from a nitronyl-nitroxide ligand and transition metal ions, Daniel O. T. A. Martins, **Cristian Andrei Spinu**, Alena Sheveleva, Mihaela Hillebrand, Floriana Tuna, Marius Andruh, *Inorganic Chemistry*, **2026**, *65*, 6544-6553.
https://doi.org/10.1021/acs.inorgchem.5c05585

IF = 4.7

Bibliography

[1] R. G. Hicks, *Org. Biomol. Chem.* **2007**, *5*, 1321-1338.

[2] D. Griller, K. U. Ingold, *Acc. Chem. Res.* **1976**, *9*, 13-19.

[3] R. G. Hicks, Stable Radicals, John Wiley & Sons Ltd, **2010**.

[4] J. H. Osiecki, E. F. Ullman, *J. Am. Chem. Soc.* **1968**, *90*, 1078-1079.

[5] E. F. Ullman, J. H. Osiecki, D. G. B. Boocock, R. Darcy, *J. Am. Chem. Soc.* **1972**, *94*, 7049-7059.

[6] B. M. Dooley, S. E. Bowles, T. Storr, N. L. Frank, *Org. Lett.* **2007**, *9*, 4781-4783.

[7] S. Suzuki, F. Nakamura, T. Naota, *Mater. Chem. Front.* **2018**, *2*, 591-596.

[8] M. Lamchen, T. W. Mittag, *J. Chem. Soc. C* **1966**, *0*, 2300-2303.

[9] S. Shimono, R. Tamura, N. Ikuma, T. Takimoto, N. Kawame, O. Tamada, N. Sakai, H. Matsuura, J. Yamauchi, *J. Org. Chem.* **2004**, *69*, 475-481.

[10] J. C. Duff, E. J. Bills, *J. Chem. Soc.* **1932**, 1987-1988.

[11] W. E. Smith, *J. Org. Chem.* **1972**, *37*, 3972-3973.

[12] Y. Ogata, A. Kawasaki, F. Sugiura, *Tetrahedron* **1968**, *24*, 5001-5010.

[13] P. Atkins, J. d. Paula, J. Keeler, Physical Chemistry, 11th Edition, Oxford University Press **2018**.

[14] J. M. D. Coey, Magnetism and Magnetic Materials, Cambridge University Press, **2009**.

[15] O. Khan, Molecular Magnetism, VCH Publishers Inc, **1993**.

[16] J. R. Gispert, Coordination Chemistry, Wiley-VCH, **2008**.

[17] R. L. Carlin, Magnetochemistry, Springer-Verlag, **1986**.

[18] S. Hatscher, H. Schilder, H. Lueken, W. Urland, *Pure Appl. Chem.* **2005**, *77*, 497-511.

[19] R. Sessoli, D. Gatteschi, A. Caneschi, M. A. Novak, *Nature* **1993**, *365*, 141-143.

[20] A. Ardavan, O. Rival, J. J. L. Morton, S. J. Blundell, A. M. Tyryshkin, G. A. Timco, R. E. P. Winpenny, *Phys. Rev. Lett.* **2007**, *98*, 057201.

[21] E. M. Pineda, D. O. T. A. Martin, F. Tuna, *Electron Paramag. Reson.* **2021**, *27*, 146-187.

[22] A. Schweiger, G. Jeschke, Principles of Pulse Electron Paramagnetic resonance, Oxford University Press, **2001**.

[23] A. Ardavan, O. Rival, J. J. L. Morton, S. J. Blundell, A. M. Tyryshkin, G. A. Timco, R. E. P. Winpenny, *Phys. Rev. Lett.* **2007**, *98*, 057201.

[24] S. Shimono, R. Tamura, N. Ikuma, T. Takimoto, N. Kawame, O. Tamada, N. Sakai, H. Matsuura, J. Yamauchi, *J. Org. Chem.* **2004**, *69*, 475-481.

[25] V. Ovcharenko, O. Kuznetsova, E. Fursova, G. Letyagin, G. Romanenko, A. Bogomyakov, E. Zueva, *Inorg. Chem.* **2017**, *56*, 14567-14576.

[26] L. Nodaraki, A. M. Ariciu, D. N. Huh, J. Liu, D. Martins, F. Ortu, R. E. P. Winpenny, N. F. Chilton, E. J. L. McInnes, D. P. Mills, W. J. Evans, F. Tuna, *J. Am. Chem. Soc.* **2024**, *146*, 15000-15009.